

# Sinking Satellites and the Heating of Galaxy Discs

Héctor Velázquez<sup>1,2,3</sup> and Simon D.M. White<sup>2</sup>

<sup>1</sup> *Institute of Astronomy, Madingley Road, Cambridge CB3 0HA, UK*

<sup>2</sup> *Max-Planck-Institut für Astrophysik, Karl-Schwarzschild-Strasse 1, D-85740 Garching bei München, Germany*

<sup>3</sup> *Observatorio Astronómico Nacional-UNAM, Apdo. Postal 877, 22800 Ensenada, B.C., México*

24 December 2018

## ABSTRACT

We have carried out a set of self-consistent N-body simulations to study the interaction between disc galaxies and merging satellites with the aim of determining the disc kinematical changes induced by such events. We explore a region of the parameter space embracing satellites with different masses and internal structure and orbits of various eccentricities. We find that the analytic estimates of Tóth and Ostriker (1992) are high; overestimating the disc heating and thickening resulting from the accretion process by a factor of about 2 – 3. We find that the heating and thickening of the disc differ for satellites on prograde and retrograde orbits. The former tend to heat the stellar disc while the latter primarily produce a coherent tilt. For instance, a satellite of a Milky Way type galaxy with an initial mass of 20% that of the disc and on a retrograde orbit increases the velocity ellipsoid at the Solar neighborhood by  $(\Delta\sigma_R, \Delta\sigma_\phi, \Delta\sigma_z)_\odot \approx (11, 9, 6)$  kms<sup>-1</sup> and produces a maximum increment of the vertical scale length and the stability parameter  $Q$  inside the solar radius of 300 pc and 0.8, respectively, increases of about 43% and 53%. The same satellite but on a prograde orbit leads to changes of  $(\Delta\sigma_R, \Delta\sigma_\phi, \Delta\sigma_z)_\odot \approx (22, 15, 12)$  kms<sup>-1</sup>,  $\Delta z_{o,\odot} \approx 550$  pc and  $\Delta Q_\odot \approx 1.2$ . Thus, disc galaxies may accrete quite massive satellites without destroying the disc, particularly, if the orbits are retrograde. We also find that a massive bulge may play a role in reducing these effects. We have quantified the importance of the responsiveness of the halo by replacing it by a rigid potential in several simulations. In these cases, the increase of the vertical scale length is larger by a factor of 1.5 – 2, indicating that a self-consistent treatment is essential to get realistic results. A frequent by-product of the accretion process is the formation of weak stellar warps and asymmetric discs. Finally, we have checked how well Chandrasekhar’s dynamical friction formula reproduces the sinking rates in several of our experiments. We find that it works well provided a suitable value is chosen for the Coulomb logarithm and the satellite mass is taken to be the mass still bound to the satellite at each moment.

**Key words:** galaxy: kinematics and dynamics – galaxies: evolution – galaxies: structure – galaxies: spiral – methods: numerical

## 1 INTRODUCTION

Most currently popular models for the formation of galaxies and larger structures postulate that growth occurs hierarchically through gravitational clustering in such a way that small objects form first and then aggregate into larger systems (Frenk et al. 1988, Carlberg and Couchman 1989, Kauffman and White 1993, Lacey and Cole 1993). The observational evidence seems to support these models since it is possible to trace the influence of merging both on galaxies

and on clusters of galaxies. We can classify mergers roughly according to the masses of the objects involved: (1) major mergers and (2) minor mergers. The first involve galaxies of comparable mass and are often invoked as a mechanism to form elliptical galaxies from spiral systems (Toomre 1977, Negroponte and White 1983, Schweizer 1990, Barnes 1992, Silk and Wyse 1993). Minor mergers involve a giant galaxy accreting a small satellite. The Large Magellanic Cloud and our own Galaxy are a clear example of such an ongoing minor merger. In spite of a general consensus that minor

mergers may drive internal evolution in galaxies, the consequences of these events are still not clear (Quinn and Goodman 1986, Quinn, Hernquist and Fullagar 1993, Walker, Mihos and Hernquist 1994 and, Huang and Carlberg 1997; hereafter QG, QHF, WMH and HC, respectively).

An important constraint on the effects of minor mergers was raised by Ostriker (1990) and Tóth and Ostriker (1992, hereafter TO). In a high density Universe dominated by cold dark matter (CDM) about 80 per cent of the dark haloes have undergone a merger in the past 5 billion years which increased their mass by 10 per cent or more (Frenk et al. 1988, Kauffman and White 1993, Navarro, Frenk and White 1994). TO argued that such a merger rate is too high to be compatible with the observed thinness and coldness of discs in spiral galaxies. Using a semi-analytic treatment of the problem, they derived an uncomfortably low upper limit for the mass that could be accreted by a disc like that of the Milky Way – no more than 4 per cent of the present mass within the solar circle could have been accreted during the last 5 billion years, given the observed local values of Toomre’s stability  $Q$ -parameter and of disc scale-height. They argued that this constraint favours a low density universe (perhaps with a cosmological constant) in which the expected merger rate is low.

Several complementary lines of investigation have been used to evaluate the argument proposed by TO. One approach concentrates on understanding the later stages of merging and the dynamical evolution of disc structure. Semi-restricted and full N-body simulations have been employed to explore how infalling satellites perturb discs (QG, TO, QHF, WMH, HC). The most recent work by WMH and HC used full N-body simulations and incorporated a key ingredient in the accretion process, the responsiveness of the halo. A possible weakness of all these studies is that they focussed on satellites on nearly circular orbits. For instance, WMH followed their satellite only after it was already within 21 kpc of the galaxy centre; this choice was imposed by their decision to use a very large number of particles (500,000) in order to reduce numerical noise and to delay the growth of a bar in their model disc. They found that accretion of a satellite with 10 per cent of the disc mass was already enough to provoke a 60 percent thickening of the stellar disc at the solar circle. In contrast, HC found that satellites with masses between 10-30 per cent of the disc mass could be put on near-circular orbits at about 10 disc half-mass radii, and would be sufficiently disrupted by tides before interacting strongly with the disc that their effects on it are quite small. The present paper is a continuation and extension of this line of research.

A complementary approach concentrates on evaluating the rate at which satellites are accreted as a function of mass and orbital parameters. Observation-based arguments can be used to estimate the current merger rate either for dark haloes or for galaxies. Thus, signs of disturbance like tidal tails and shells can be considered signs of a recent merger and thus allow the merger rate of luminous galaxies to be obtained. From a sample of 4000 galaxies, 10 were identified by Toomre (1977) as results of a recent merger. From this he was able to derive a lower limit of  $0.005 \text{ Gyr}^{-1}$  for the cur-

rent merger rate. A higher merger rate of about  $0.04 \text{ Gyr}^{-1}$  was found by Carlberg, Pritchet & Infante (1994) based on the observed numbers of close galaxy pairs and the assumption is that pairs will merge if their closest approach distance and relative velocity are less than their characteristic radius and their internal velocity dispersion, respectively (Aarseth and Fall 1980). On larger scales it is clear that substructure is a common feature of clusters of galaxies, suggesting that many of them have formed recently by the merging of several smaller systems (Dressler and Shectman 1988; Jones and Forman 1992; Richstone, Loeb and Turner 1992). Using another version of the TO argument, the observed amount of substructure in clusters can give an estimate of the current merging rate and so of the cosmic density parameter  $\Omega$  (Richstone, Loeb and Turner 1992; Lacey and Cole 1993; Kauffman and White 1993; Evrard et al. 1994). Neither of these arguments, however, can give the satellite accretion rates needed to evaluate the TO argument.

Satellite accretion rates can be estimated from theoretical arguments based either on the Press-Schechter model for hierarchical clustering (Lacey and Cole 1993) or on high resolution simulations. For example, Navarro, Frenk and White (1994, 1995) have carried out a series of simulations of the formation of galaxy-satellite systems in an  $\Omega = 1$  CDM universe; their results suggest that the existence of thin discs may, perhaps, be reconciled with such a model, because discs are less efficient at accreting material than are their surrounding dark haloes. In these simulations fewer than 30 per cent of the discs grew by more than 10 per cent in mass over the last 5 Gyr, whereas about 80 of the haloes grew by this much or more. The distributions of orbital orientation and orbital eccentricity of their satellites were essentially uniform. Thus, Lacey and Cole’s (1993) suggestion that the TO constraint might be avoided if satellites are primarily on near-circular orbits does not seem to be viable in a realistic hierarchical clustering model. Note that while the simulations of Navarro et al. (1995) give useful indications about the rates of satellite accretion onto discs, their resolution is too low to give information about how this accretion affects disc structure.

In the present paper we address the heating of the stellar disc by infalling satellites following the first approach discussed above. We consider satellites with a variety of internal structures and on orbits with a variety of initial orientations and eccentricities. We follow the evolution of the systems by using full N-body simulations of all the components. Our paper is organized as follows: section 2 contains brief descriptions of the models we adopt for our primary and satellite galaxies, of our numerical methods, and of the parameters of the set of simulations we have carried out. Section 3 studies how the disc is heated and thickened by infalling satellites and a comparison with TO’s results is given in section 4. We discuss the tilting and warping of the disc resulting from such events in section 5. Section 6 concentrates on the disruption of the satellite and the evolution of its orbit. We show, in section 7, that the latter can be well reproduced by Chandrasekhar’s local formulation of dynamical friction. In section 8 we replace our “live” halo by a rigid one to demonstrate how halo response affects the accretion and disc heating processes. Finally, in section 9,

**Table 1.** Galactic parameters.

	Symbol	Value
Disc:		
	$N_D$	40 960
	$M_D$	$5.6 \times 10^{10} M_\odot$
	$R_D$	3.5 kpc
	$z_o$	700 pc
	$Q_\odot$	1.5
	$R_\odot$	8.5 kpc
	$\epsilon_D$	175 pc
Bulge:		
	$N_B$	4 096
	$M_B$	$1.87 \times 10^{10} M_\odot$
	$a^*$	525 pc
	$\epsilon_B$	175 pc
Halo:		
	$N_H$	171 752
	$M_H$	$7.84 \times 10^{11} M_\odot$
	$\gamma$	3.5 kpc
	$r_{cut}$	84 kpc
	$\epsilon_H$	175 pc

\* The bulge half-mass radius is 1.27 kpc.  $N_D$ ,  $N_B$  and  $N_H$  correspond to the number of particles used for each galaxy component. The system of units is such that  $G = M_D = R_D = 1$ .

we summarize our main conclusions.

## 2 NUMERICAL PRELIMINARIES

In this section we describe briefly the idealised models which we adopt to describe the primary disc galaxy and the satellites which merge with it. We also describe the numerical tools employed to follow the dynamical evolution of the primary/satellite system, and the parameters which define the specific set of simulations which we have carried out.

### 2.1 The Primary Galaxy Model

We use the methods of Hernquist (1993) to set up a self-consistent N-body realization of a galaxy model consisting of three components: a disc, a bulge and a halo. A detailed description of the technique can be found in Hernquist's paper. The density distributions of the three components are:

$$\rho_D(R, z) = \frac{M_D}{4\pi R_D^2 z_o} \exp(-R/R_D) \operatorname{sech}^2(z/z_o), \quad (1)$$

$$\rho_B(r) = \frac{M_B}{2\pi} \frac{a}{r(a+r)^3}, \quad (2)$$

$$\rho_H(r) = \frac{M_H \alpha}{2\pi^{3/2} r_{cut}} \frac{\exp(-r^2/r_{cut}^2)}{r^2 + \gamma^2}. \quad (3)$$

Here,  $M_D$ ,  $M_B$  and  $M_H$  correspond to the masses of the disc, the bulge and the halo, respectively.  $R_D$  and  $z_o$  are the radial and vertical scale lengths of the disc.  $a$  defines the scale length of the bulge and corresponds to a half-mass radius of  $a(1 + \sqrt{2})$  (Hernquist 1990). Finally,  $\gamma$  and  $r_{cut}$  are

the core and cut-off radii for the halo and  $\alpha$  is a normalisation constant. Notice that we assume both the bulge and the halo to be spherical.

The velocities are derived from the Jeans equations (e.g. Binney and Tremaine 1987). Isotropic gaussians are assumed for the halo and bulge velocity distributions. For the disc, the square of the radial velocity dispersion is taken to be proportional to the surface density of the disc,  $\sigma_R^2 \propto \exp(-R_D/R)$  (Lewis and Freeman 1989) and the vertical component of the velocity ellipsoid is determined from  $\sigma_z^2 = \pi G \Sigma(R) z_o$  in agreement with an isothermal sheet (Spitzer 1942). The azimuthal component is obtained from the epicyclic approximation,  $\sigma_\phi^2 = \sigma_R^2 \kappa^2 / (4\Omega^2)$ . Finally, the constant of proportionality is determined by fixing the value of Toomre's stability Q-parameter to a given value. We select  $Q_\odot = Q(R_\odot) = 1.5$  at the Solar radius.

We have chosen a system of units such that  $U_m = M_D = 1$ ,  $U_l = R_D = 1$  and  $G = 1$ . For a disc mass of  $5.6 \times 10^{10} M_\odot$  and a disc radial scale length of 3.5 kpc (Bahcall, Schmidt and Soneira 1983) the units of time and velocity are  $1.3 \times 10^7$  yr and  $262 \text{ kms}^{-1}$ , respectively. The half-mass radius of the disc is  $\sim 1.7 R_D$  with a rotation period at this radius of about 13 time units. The model can be easily scaled through the following expressions for the time and velocity units:

$$U_t = 4.709 \times 10^{11} \left( \frac{U_l^3}{U_m} \right)^{1/2} \text{ yr} \quad (4)$$

$$U_v = 2.076 \times 10^{-3} \left( \frac{U_m}{U_l} \right)^{1/2} \text{ kms}^{-1} \quad (5)$$

where  $U_m$  and  $U_l$  are given in solar masses and kpc, respectively. In Table 1 we summarize the values of the parameters that define our primary galaxy model.

We should notice that (1) our halo is probably too small to be realistic. Studies of satellites in the Local Group and around external galaxies show that galactic haloes extend to radii beyond 200 kpc with masses exceeding  $2 \times 10^{12} M_\odot$  (Zaritsky et al. 1989, Zaritsky and White 1994). However, our halo is consistent with the largest velocities observed for halo stars in the solar neighborhood (Carney and Latham 1987) and should be massive enough to give realistic orbital velocities for eccentric satellite orbits. (2) Our halo is maybe too concentrated. Persic, Salucci and Stel (1996) argue for a halo core radius of about  $1 - 2 R_{opt}$  where  $R_{opt} = 3.2 R_D$  is the optical radius. However, a model with such a halo will be prone to form a bar which is an undesirable additional source of disc heating and to prevent its growth it will be necessary to increase the bulge contribution. The values of the parameters listed in Table 1 guarantee stability against bar formation of the disc galaxy model in isolation (Velázquez and White, in preparation).

The rotation curve of our galaxy model (solid lines) is shown in figure 1. For comparison, two other rotation curves are displayed for different bulge masses but with the same disc and halo. The rotation curve for our galaxy model at the optical radius is  $V_C(R_{opt}) \approx 243 \text{ kms}^{-1}$  in model units while the models with a bulge mass of  $M_B = 0.2 M_D (= 1.12 \times 10^{10} M_\odot)$  and  $M_B = 2/3 M_D (= 3.73 \times 10^{10} M_\odot)$  have values of  $V_C(R_{opt}) \approx 236 \text{ kms}^{-1}$  and  $V_C(R_{opt}) \approx 257$

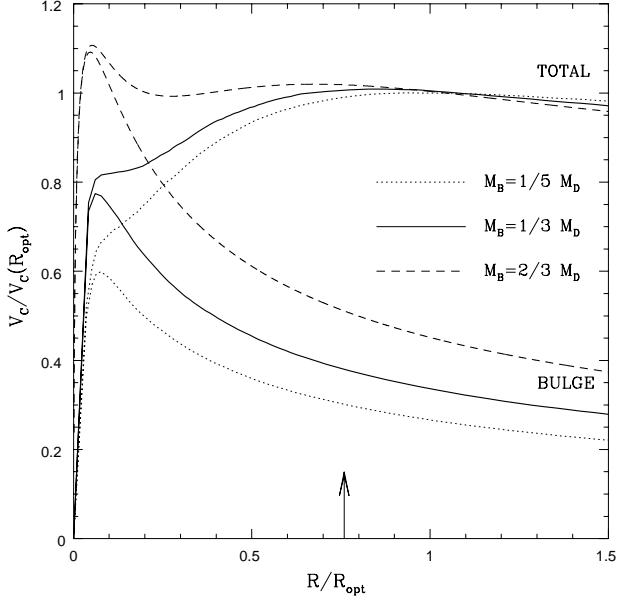


**Figure 1.** The rotation curve for our disc galaxy model (solid lines) has a value of  $V_C(R_{opt}) \approx 243 \text{ kms}^{-1}$  where  $R_{opt} = 3.2 R_D$ . Dotted-lines and dashed-lines correspond to rotation curves for bulge masses of  $0.2 M_D$  and  $2/3 M_D$  with values of  $V_C(R_{opt}) \approx 236 \text{ kms}^{-1}$  and  $V_C(R_{opt}) \approx 257 \text{ kms}^{-1}$ , respectively. For clarity the contribution of the disc and halo are not shown. The arrow indicates the Solar position.

$\text{kms}^{-1}$ , respectively. We can observe that, at difference of the sample of rotation curves given by Persic et al. (1996), the rotation curve of our model shows a steeper rise in the inner region which is consistent with the observed nuclear rotation curves of galaxies in the CO-line emission and with the optical rotation curves for large bright galaxies (Sofue et al. 1997, Courteau 1997). Furthermore, it peaks near  $R_{opt}$  in agreement with the results of Courteau (1997).

Finally, we should mention that for this galaxy model we have used a total number of 216 808 particles. Most of these are in the halo component (171 752) where large numbers are required to reduce heating of the disc by two-body relaxation effects.

## 2.2 Satellite Models

The satellites are represented by self-consistent King models (King 1966) which provide a reasonable fit to early-type and nucleated dwarf galaxies (Vader and Chaboyer 1994). These models are a sequence of truncated isothermal spheres parametrized by a concentration  $c \equiv \log_{10}(r_t/r_c)$ , where  $r_t$  and  $r_c$  are the so-called tidal and core radii, respectively. To specify completely a satellite model we provide the satellite mass,  $M_S$ , its concentration and its tidal radius. The latter is estimated from the density contrast  $\rho_S(r_t)/\bar{\rho}_G(r_a) \sim 3$  at the apocentric distance,  $r_a$ , of the orbit where the satellite is initially placed. The parameters that characterize our satellite models, including the central density and the central one-dimensional velocity dispersion, are listed in Table

**Table 2.** Satellite models.

Model	Symbol	Value
S1:		
$M_S$		$5.60 \times 10^9 M_\odot$
$r_c$		1 kpc
$c$		0.8
$\rho_c$		$0.52 M_\odot/\text{pc}^3$
$\sigma_c$		$52 \text{ kms}^{-1}$
S2:		
$M_S$		$5.60 \times 10^9 M_\odot$
$r_c$		500 pc
$c$		1.1
$\rho_c$		$0.84 M_\odot/\text{pc}^3$
$\sigma_c$		$60 \text{ kms}^{-1}$
S3:		
$M_S$		$1.12 \times 10^{10} M_\odot$
$r_c$		875 pc
$c$		1
$\rho_c$		$1.36 M_\odot/\text{pc}^3$
$\sigma_c$		$71 \text{ kms}^{-1}$

$c$  defines the concentration of the satellite model and is given by  $\log_{10}(r_t/r_c)$  where  $r_c$  and  $r_t$  are, respectively, the core and tidal radii of a King model.  $M_S$ ,  $\rho_c$  and  $\sigma_c$  denote the satellite mass, the central density and the central one-dimensional velocity dispersion, respectively.

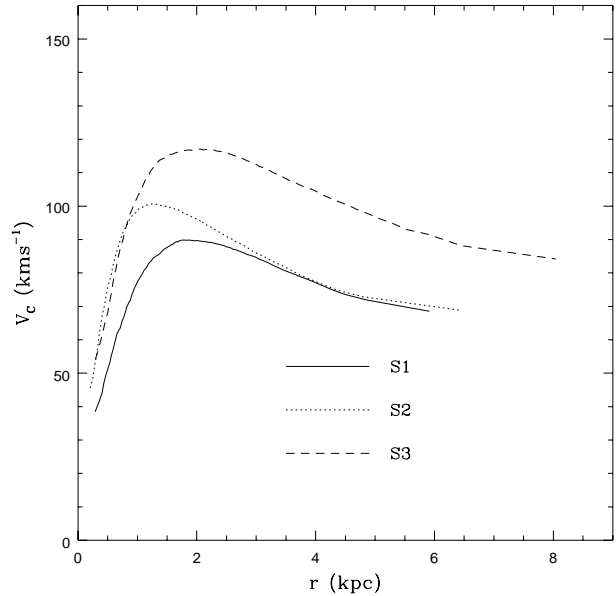


**Figure 2.** Rotation curve for our satellite models.

2 which are within the observed values (Vader and Chaboyer 1994; Binggeli and Cameron 1991; Bender, Burstein and Faber 1992). The rotation curve for each satellite model is shown in figure 2. We can notice that our satellite models are more concentrated than DD154-type dwarf galaxies (Moore 1994). In all cases, the satellite consists of 8192 particles.

**Table 3.** Simulations.

Name	Sat. model	$\theta_i$	$\epsilon_J$	$r_p/R_D$	$r_a/R_D$
G1S1	S1	45°	0.33	1.5	16.86
G1S2	S1	0°	0.55	3	15.71
G1S3	S1	45°	0.55	3	15.71
G1S4	S1	90°	0.55	3	15.71
G1S5	S1	135°	0.55	3	15.71
G1S6	S1	180°	0.55	3	15.71
G1S7	S1	0°	0.82	6	13.29
G1S8	S1	45°	0.82	6	13.29
G1S9	S2	0°	0.55	3	15.71
G1S10	S2	45°	0.55	3	15.71
G1S11	S2	90°	0.55	3	15.71
G1S12	S2	135°	0.55	3	15.71
G1S13	S2	180°	0.55	3	15.71
G1S14	S3	45°	0.55	3	15.71
G1S15	S3	135°	0.55	3	15.71

$\theta_i$  refers to the angle between the initial angular momentum of the satellite and the initial angular momentum of the disc.  $\epsilon_J$  defines the circularity of the orbit,  $r_p$  and  $r_a$  correspond to the initial pericentric and apocentric radii of the orbit, respectively.

### 2.3 Numerical Methods and Orbital Parameters

To follow the evolution of the galaxy-satellite system we use a tree algorithm with a tolerance parameter of  $\theta_{\text{tol}} = 0.75$  and an integration timestep of  $1.3 \times 10^6$  yrs. Forces between particles are computed including the quadrupole components (see Barnes and Hut (1986) and Hernquist (1987) for details of this code). With these values, the conservation of global energy and angular momentum is better than 1 per cent for all our models.

Since our initial galaxy and satellite models are not in a perfect equilibrium we allow them to relax separately before starting an interaction simulation. The disc galaxy is relaxed for 20 time units, about one and a half rotation periods at its half-mass radius, while the satellite is allowed to evolve for 40 time units to reduce initial transient effects. These two configurations are then superposed to create our initial conditions. We have performed a set of experiments varying the parameters that are likely to influence the result of a galaxy-satellite interaction, for example, the ‘circularity’ of the orbit, the angle between the angular momentum of the satellite and the disc, and the satellite structure. In Table 3 we list the parameters of these simulations. Here, the ‘circularity’ of the orbit has been defined as  $\epsilon_J \equiv J/J_C(E)$ , where  $J$  is the angular momentum of the satellite and  $J_C(E)$  is the corresponding angular momentum for a circular orbit of the same energy  $E$  as the satellite’s orbit. Also, we have followed the subsequent evolution of the galaxy model in isolation (our control model) to distinguish effects produced by two-body encounters from those provoked by the accretion of the satellite. The discussion of the following sections all refers to satellites on orbits which actually intersect the disc.

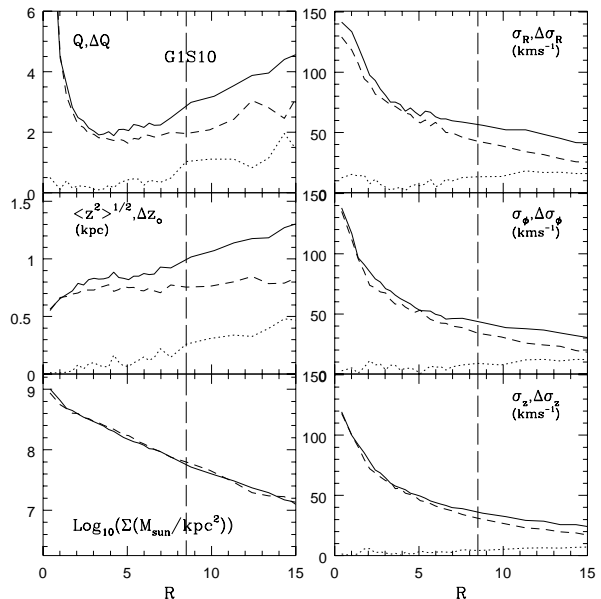


**Figure 5.** The kinematical properties of the disc in our model G1S10. Solid lines give the kinematics of the disc in this model after 3.3 Gyr, while short-dashed lines show corresponding quantities for our control model. Dotted lines show the difference between the two, and so the part of the changes due purely to the interaction. In all plots the vertical long-dashed line indicates the position at  $R_\odot$ .

### 3 DISC HEATING AND THICKENING

In figures 3 and 4 we show the evolution of the disc of our models G1S10 and G1S12 (see Table 3). At the end of these simulations the satellite has been completely disrupted and the disc component has been altered in three different ways: (1) it is hotter and thicker; (2) it is no longer axisymmetric; and (3) it is tilted and warped. We discuss some of these effects in this and the following sections.

To determine the kinematics of the disc we rotate to axes aligned with the principal axes of the disc inertia tensor and then average particle properties in concentric cylindrical annuli. These averages are a crude measure of the disc kinematics since warping and azimuthal asymmetry are not taken into account. The heating and thickening of the disc can be described by the changes of the velocity dispersions ( $\Delta\sigma_R, \Delta\sigma_\phi, \Delta\sigma_z$ ) and by the increase of the vertical scale length,  $\Delta z_o$ . Effects due to two-body relaxation can be subtracted by comparing the final state to that of the control model. The increase of Toomre’s stability parameter,  $Q$ , is also shown. We compute the vertical scale length in each annulus using the following definition  $z_o(R) \equiv \langle z^2 \rangle^{1/2}$ .

In figure 5 we show the disc kinematical properties of our model G1S10 (solid lines) together with the corresponding properties of the control model (short-dashed lines). It is evident from this figure that thickening of the stellar disc does not occur uniformly at all radii; regions beyond  $R_\odot$  are much more susceptible to damage by the infalling satellite than the inner disc. Given the complexity of the final disc structure we found it convenient to sample the kinematics

**Figure 3.** The evolution of the disc for model G1S10. A fourth of the total number of disc particles has been plotted. The satellite has been tidally disrupted at time 252. By this time, the disc has been slightly tilted and shows an asymmetric configuration (see text for a discussion of some of these issues).

at three representative radii: near the centre (averaged out to  $\sim 2$  kpc), at  $R_{\odot}$ , and at 14 kpc. This is sufficient to provide us with a global view of the heating and thickening. In Table 4 we give the final disc structure at these radii for all our simulations listed in Table 3\*. For example, the velocity ellipsoid of the disc in model (G1S10) grows by (18, 12, 8)

\* Satellite particles are not considered in computing the kinematical properties of the disc because, in most of the cases, their orbits do not fall into the disc plane and so they would be separated from disc particles by their kinematics. Particles from satellites on prograde coplanar orbits would be more difficult to distinguish, however, in these simulations they form a disc-like structure with a hole of about 3–4 kpc in the central region (see also Barnes 1996).

$\text{kms}^{-1}$ , (12, 10, 5)  $\text{kms}^{-1}$  and (19, 14, 8)  $\text{kms}^{-1}$  (from inside to outside) resulting in increases of Toomre’s  $Q$  parameter by about 0.4, 0.8 and, 2.2. Before the accretion event  $Q$  was roughly constant between 3 kpc and 9 kpc with a value of  $\sim 1.5$  and after satellite accretion it has risen to  $Q \sim 2$  between 3 kpc and 7 kpc. The vertical scale length in this same case increases by 100 pc, 275 pc and 500 pc, representing a thickening by about 14, 39 and, 71 per cent; while for its retrograde counterpart (model G1S11) is of 21, 21 and 43 per cent. Disc thickening is even lower for model G1S3 being of 7, 14 and 43 per cent (see entries in Table 4). In some of the models (G1S5, G1S10, G1S12 and G1S14) satellite accretion induces additional heating and thickening by exciting a bar-like instability in the inner 5 kpc.

**Figure 4.** The disc evolution for the retrograde counterpart of figure 3 (see model G1S12 in Table 3). The disc looks thicker than it really is because of tilting.

Three main trends are observed in our simulations: (1) a mighty correlation between the change in disc structure and the relative orientation of disc and satellite angular momenta. We find that, in general, the disc is much more susceptible to damage by a satellite on a prograde orbit than by its retrograde counterpart. This suggests a resonant coupling between satellite orbit and disc. This difference is most clearly seen by comparing the entries in Table 4 for the coplanar prograde case (model G1S9) and the corresponding polar case (model G1S11). In figure 6, we illustrate these effects using our two simulations with massive satellites (G1S14 and G1S15 in Table 3). Notice that for the retrograde case the disc is less strongly affected at all radii. (2) In general, the planar components of the velocity ellipsoid respond more strongly than the vertical component to the accretion of the satellite. Indeed, the ratio of the two

planar components is fixed by epicyclic theory. The degree of anisotropy is correlated with both the inclination and the sense of motion of the orbit, being greatest for prograde coplanar orbits. As a result Toomre’s stability parameter  $Q$  responds more sensitively than the vertical scale length to the accretion event. This is largely a consequence of the fact (addressed in section 5) that vertical perturbations tend to tilt the disc rather than to heat it. (3) For our model G1S3 the effects of accretion on the disc are quite modest, but a more massive and compact satellite can have a very large effect (see entries of model G1S3 and G1S14 in Table 4).

**Table 4.** Disc kinematical changes.

Model	$R_c^*$			$R_\odot$			$R_4^\dagger$		
	$(\Delta\sigma_R, \Delta\sigma_\phi, \Delta\sigma_z)$ (kms $^{-1}$ )	$\Delta Q$	$\Delta z_o$ (pc)	$(\Delta\sigma_R, \Delta\sigma_\phi, \Delta\sigma_z)$ (kms $^{-1}$ )	$\Delta Q$	$\Delta z_o$ (pc)	$(\Delta\sigma_R, \Delta\sigma_\phi, \Delta\sigma_z)$ (kms $^{-1}$ )	$\Delta Q$	$\Delta z_o$ (pc)
G1S1	(9, 6, 4)	0.3	50	(5, 3, 2)	0.5	150	(10, 7, 4)	1.2	225
G1S2	(16, 8, 4)	0.4	75	(16, 10, 4)	1.1	200	(32, 21, 6)	2.6	300
	[(16, 7, 5)]	[0.5]	[100]	[(31, 12, 4)]	[1.4]	[200]	[(47, 26, 9)]	[2.9]	[450]
G1S3	(10, 7, 5)	0.3	50	(5, 3, 2)	0.5	100	(11, 6, 5)	1.4	300
G1S4	(12, 6, 4)	0.5	100	(4, 3, 2)	0.4	100	(6, 5, 4)	0.9	250
G1S5 $^\ddagger$	(24, 16, 8)	0.6	200	(4, 2, 3)	0.5	100	(6, 6, 4)	1.0	150
G1S6	(6, 5, 7)	0.3	75	(5, 4, 3)	0.4	100	(10, 7, 5)	1.7	275
G1S7	(38, 18, 8)	0.4	100	(16, 12, 5)	1.2	250	(27, 14, 7)	3.4	450
	[(38, 17, 9)]	[0.4]	[100]	[(15, 12, 6)]	[1.1]	[250]	[(29, 16, 8)]	[3.4]	[500]
G1S8	(10, 10, 6)	0.3	50	(10, 7, 4)	0.8	150	(17, 12, 6)	2.2	350
G1S9	(19, 13, 11)	0.5	100	(22, 15, 7)	1.5	300	(37, 23, 9)	2.6	550
	[(19, 13, 11)]	[0.5]	[100]	[(25, 15, 8)]	[1.6]	[350]	[(43, 28, 12)]	[2.9]	[675]
G1S10 $^\ddagger$	(18, 12, 8)	0.4	100	(12, 10, 5)	0.8	275	(19, 14, 8)	2.2	500
G1S11	(11, 10, 6)	0.4	100	(7, 4, 4)	0.5	150	(11, 8, 5)	1.0	300
G1S12 $^\ddagger$	(17, 11, 11)	0.8	150	(4, 4, 4)	0.4	150	(10, 6, 6)	1.0	300
G1S13	(7, 8, 4)	0.5	75	(12, 10, 7)	0.8	250	(19, 15, 10)	2.4	700
G1S14 $^\ddagger$	(32, 20, 12)	0.6	150	(22, 15, 12)	1.2	550	(27, 18, 16)	2.9	800
G1S15	(20, 12, 8)	0.6	100	(11, 9, 6)	0.8	300	(21, 12, 10)	2.2	525

Symbols \* and † denote quantities at the centre and  $4R_D$ , respectively. Models forming a bar are indicated by the symbol ‡. Quantities in brackets are computed by taking into account satellite particles.

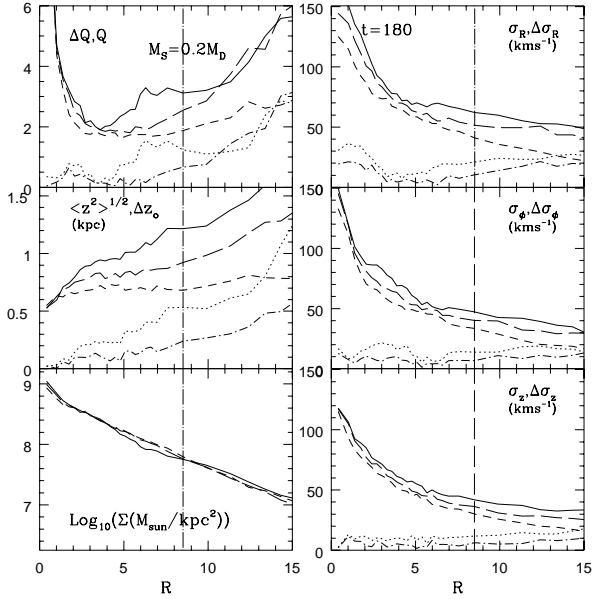


**Figure 6.** The response of the disc to the infall of a satellite with an initial mass of  $0.2 M_D$ . The satellite at this time (2.34 Gyr) has been completely destroyed. The solid lines correspond to a satellite following a prograde orbit with initial angle of  $\theta_i = 45^\circ$ , (G1S14) while the long-dashed lines correspond to its retrograde counterpart (G1S15) with  $\theta_i = 135^\circ$ . For reference, the kinematical structure in our isolated control model is also shown (short-dashed lines). The kinematical changes for model G1S14 are indicated by dotted lines and for model G1S15 by dashed-dotted lines. The vertical line again indicates the position at the Solar radius.

### 3.1 Disc Heating and the Bulge/Disc Mass Ratio

To address the effect of the bulge in the heating process of the stellar disc we have repeated a few of our simulations but with two additional galactic models. One of them has a bulge with a mass of  $M_B = 0.2 M_D$  and the other with a mass of  $M_B = 2/3 M_D$ . We did not pursue a larger reduction of the bulge mass since it requires a huge number of particles ( $> 5 \times 10^5$ ) to keep stable the disc against bar formation during the disruption times in our simulations; this would be prohibitive (e.g. Walker et al. 1996). In these models both the disc and halo are the same as in our primary galaxy model of section 2. In figure 1 we show the rotation curves for these new galactic models.

In Table 5 we summarize the disc kinematical changes for these new experiments. Prefix G2 and G3 refer to the galactic model with the less and more massive bulge, respectively. We should mention that model ‘G2’ develops a bar in isolation at time  $\sim 3.2$  Gyr inside 4 kpc. Comparing the entries in tables 4 and 5 at the Solar radius we can see that the disc has been thickened by 39, 39 and 21 per cent for models G1S10, G2S10 and G3S10, respectively, while for their retrograde counterparts (G1S12, G2S12 and G3S12) the corresponding values are only of 21, 29 and 14 per cent. This suggest that a very massive bulge would be more efficient in reducing the heating and thickening of the stellar disc. This effect can be more clearly appreciated in our models with the more massive satellite (models G1S14, G1S15, G3S14 and G3S15). Thus, the difference between the thickening found by Walker et al. (1996) ( $\sim 60\%$ ) and that in our simulations can be attributed to the fact that in the former case the satellite interacts strongly with the disc because of the orbit chosen and because of the bulgeless galaxy model.

The latter forms a bar during the early stages of the accretion.

#### 4 COMPARISON WITH TO'S RESULTS

It is interesting to compare the size of the effects we find with those predicted analytically by TO. They give formulae for the changes in the disc vertical scale length, velocity dispersions and stability parameter  $Q$  (their equations 2.16, 2.21, 2.25 and 2.26). These can be used to estimate the quantities we list in Table 4 and 5. We apply these formulae by inserting the properties of the unperturbed disc (as measured in our control model) at the Solar radius and the satellite total mass, and by averaging over the orbital inclination of the satellite. In figure 7, we show the resulting disc changes as predicted by TO (solid and dashed lines for two extreme cases) together with those found in our simulations (denoted by starred symbols). The solid lines correspond to a vertical ( $\epsilon_{\perp}$ ) and epicyclic ( $\epsilon_{\parallel}$ ) efficiency heating assuming circular orbits with random inclinations for the velocity distribution of the satellites while the dashed lines refer to an isotropic Maxwellian distribution (see TO, Appendix A). Clearly, the analytical predictions tend to overestimate the disruptive effects of satellite accretion by a non-negligible factor; typically about 2–3. These differences are more marked for the more massive satellite. Notice that for models G1S2, G1S7 and G1S9 the change in the stability parameter is closer to that predicted by TO. This is because the satellite in these models (which follows a prograde orbit near the disc plane) induces substantial deviations in  $\Sigma_D(R)$ . These deviations were taken into account in determining the change in  $Q$  for figure 7. If we ignore such variations, as TO did, then  $\Delta Q$  is entirely determined by  $\Delta\sigma_R$ ; the difference is then more dramatic since the change in  $Q$  is reduced to 0.8, 0.7 and 1.0 for models G1S2, G1S7 and G1S9, respectively.

The fact that we find substantially weaker effects than those predicted by TO suggests that their limits on the accretion rate of satellites (based on the thinness of observed discs, and their susceptibility to spiral instabilities) are likely to be too strict. There are some additional effects which may result in our own results still being a significant overestimate of the extent of the damage.

- The stellar dynamical heating of the disc in our simulations may be partially compensated by dissipative effects in a gaseous component. N-body/Hydrodynamical simulations carried out by Mihos and Hernquist (1994) and the recent work by HC reveal that gas cooling can make an important contribution to sustaining spiral structure in galaxies.

- Our simulations begin with the satellite already quite close to the disc and have relatively low mass halos. They are thus likely to underestimate disruptive effects on the satellite before it begins to interact strongly with the disc (see HC). Progress on this point will require larger simulations and properly realistic “cosmological” initial conditions. Currently available results suggest that discs may accrete material less efficiently than haloes (NFW94, NFW95).

- Damaging effects on disc structure will be diminished whenever the satellite is less concentrated than those we have considered and so can be disrupted before encountering

the disc (again see HC). Although simulations from cosmological initial conditions show that the distribution of orbital eccentricities should be almost uniform so that a significant fraction of satellites reach the disc essentially unperturbed on their first passage, such high velocity, near-radial encounters cause less damage than prograde encounters at lower velocities.

It is interesting that the properties of the most strongly perturbed discs in our simulations do seem to agree with those of the thick disc component at the solar radius. This component has a velocity ellipsoid of about  $(63, 42, 38)$   $\text{kms}^{-1}$ , a vertical scale length of 1 kpc and an asymmetric drift of about  $25 \text{ kms}^{-1}$  (Freeman 1996). Similar structure can be seen in the galaxy NGC 4565 for which the vertical scale length is  $\approx 1.5$  kpc (Morrison 1996).

The difference between TO's analytical results and those of our simulations may be due to one or a combination of the following factors:

- A self-gravitating satellite has the capacity to absorb part of its orbital energy which can be carried away by the stripped material. In this way, the deposition of energy onto the disc is diminished.
- Another important ingredient in the galaxy-satellite interaction is the responsiveness of the halo. This regulates the transfer of angular momentum between the different components and may weaken the resonant response of the disc to the infalling satellite.
- In addition, TO do not make any distinction between satellites on prograde and retrograde orbits and this has important consequences for the survival and evolution of the disc (see section 3 and 5).
- Another controversial point in TO's derivation is their assumption that the deposition of a satellite's orbital energy in the disc is a local process. They argued that the overall energy change in the disc would be the same if the excitation of modes in the disc were taken into account, but the formation of spirals and warps reveals that *global* modes are excited by the infalling satellite before it crosses the main disc.

#### 5 DISC TILTING AND WARPING

As the satellite sinks to the galactic centre it transfers energy and angular momentum to its surroundings (QHF, HC). Part of this energy, as we saw in section 3, goes to the disc in random vertical motions giving rise to the disc thickening. There is also, however, a coherent response of the disc to the satellite accretion which is associated with the tilting observed in figures 3 and 4. Looking in figure 8 we can also appreciate the effect of the orbital type, compactness and mass of the satellite and the mass of the bulge on the evolution of the vertical kinetic energy. The solid line corresponds to the vertical heating of the disc component coming from numerical relaxation while the starred symbols refer to the vertical kinetic energy as measured in a reference frame that coincides with the main axes of the inertia tensor and the open circles correspond to the vertical kinetic energy in the original reference frame. We can appreciate some general trends: (i) In the prograde models most of the energy goes



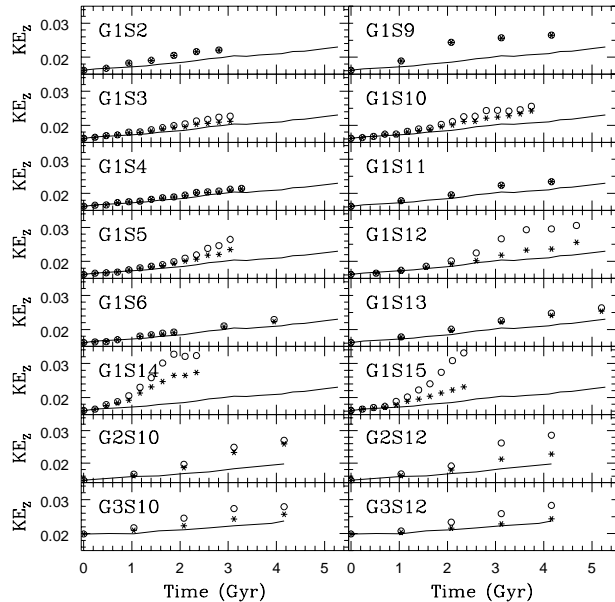


**Figure 8.** Evolution of the vertical kinetic energy of the disc for several of our models. The solid line represents the vertical heating produced by numerical relaxation. The starred symbols refer to the vertical kinetic energy as measured from a frame that coincides with the main axes of the inertia tensor while the open circles show its evolution in the initial reference frame.

duce the vertical heating of the disc which is more dramatic in models G1S10, G2S10 and G3S10 but this is not the case in their retrograde counterparts for which the coherent response of the disc seems to be reduced (e.g. models G1S12, G2S12 and G3S12).

In the absence of a satellite there is a small exchange of angular momentum between the disc and the halo resulting in a small tilt of the disc, less than  $3^\circ$  over  $\sim 4.5$  Gyr. When a satellite is introduced in the galaxy, the transfer of angular momentum changes dramatically. By the end of the simulation, the disc of model G1S14 has been tilted by  $\sim 11^\circ$  while the angle  $\theta_i$  (for both bound and unbound satellite particles) has fallen by  $\sim 26^\circ$  from its initial value. For model G1S15, the disc has been tilted by  $\sim 15^\circ$ , which, as noted above, is larger than for the corresponding prograde case. In this last model, the angle  $\theta_i$  remained almost unchanged which tells us about the importance of the coupling between disc stars and the satellite orbit. However, in both cases about 45 per cent of the total initial angular momentum of the satellite remains in the satellite debris, the rest going to the disc and the halo. Less massive satellites experience less dramatic evolution since the sinking rate and, hence, the loss of angular momentum is proportional to the square of the satellite mass. Thus, in our models G1S3 and G1S5 about 61% and 68%, respectively, of the angular momentum remains in the satellite debris. Also the disc tilting is only about  $6^\circ$  and  $8^\circ$  in these cases.

On the other hand, observations of edge-on disc galaxies show that a considerable fraction of them have a conspicuous feature in the form of an ‘integral sign’, commonly known

as a warp. Most of these structures develop far beyond the optical disc and are very extended (Briggs 1990). A typical example is our own Galaxy for which the HI warp, detected at 21 cm, is revealed beyond the solar circle (Henderson et al. 1982). However, HI warps are observable mainly where the optical disc ends and the detection of stellar warps is harder. A systemic attempt was made by Sánchez-Saavedra, Batañer and Florido (1990) by selecting a sample of 82 edge-on disc galaxies from the Palomar Survey. They were able to identify 23 cases of stellar warps in that sample. This study suggests that stellar warps are also a common feature, but their origin remains a puzzle.

From a theoretical perspective, several scenarios have been proposed to try to explain the origin of the warping of disc galaxies (an excellent review on the subject is found in Binney 1992). Among the most frequently invoked is a cosmological origin reflecting the time when the galaxy was built up. Current cosmological simulations suggest that dark haloes are highly flattened with mean axis ratios of  $\langle c/a \rangle \sim 0.5$  and  $\langle b/a \rangle \sim 0.7$  (Dubinski and Carlberg 1991). As a consequence, the disc angular momentum may not be in alignment with one of the main halo axes which may then induce a warping mode in the disc. This tilting mode was studied by Sparke and Casertano (1988) for the case of a disc embedded in a flattened rigid halo; they found that it is consistent with observed warps. However, recent self-consistent N-body simulations carried out by Dubinski and Kuijken (1995) have shown that the response of the halo can not be ignored, since dynamical friction can damp the warps in much less than a Hubble time. Nelson and Tremaine (1995) used perturbation theory to arrive at a similar conclusion, suggesting that, in general, a primordial origin of galactic warps may be ruled out.

Another mechanism to excite and maintain warps resorts to the accretion of satellites (Binney 1992) which has been highlighted in a recent paper by Weinberg (1996). This last author has shown the importance of the response of the halo (assumed spherical) of our Galaxy to the interaction with the LMC, and its subsequent effect on the formation of the disc’s HI warp. Since in all our simulations the halo is assumed spherical we can address the relevance of such events in the formation of stellar warps. For this, we proceeded by rotating our disc along the main axes of the inertia tensor of the particles located inside  $3R_D$  and representing it by a system of initially concentric rings equally spaced and each containing a sufficient number of particles. This done, each ring is displaced to a new centre determined by the centre of mass of the particles within it. Finally, we compute the inertia tensor for each ring and rotate to its principal axes. Figure 9 shows the result of this process for our isolated galaxy model ‘G1’ (upper panel) and for our models G1S3, G1S8 and G1S14, respectively. The size of the each box is  $56 \times 56 \times 3.5$  in kpc. We can see that model G1S3 produces no distinguishable warp while a more massive satellite (model G1S14) in the same orbit or a satellite on a more nearly circular orbit (model G1S8) produces bigger changes. However, it is important to remark that even in the most favorable case the departure of the warp from the disc plane is less than 1.75 kpc in the outer parts which correspond to an

**Figure 9.** Representation of the disc by a set of rings equally spaced in the polar radius. Each ring has been displaced to the centre defined by the centre of mass of the particles contained in it and then rotated to the principal axes of its inertia tensor. The size of the boxes are  $56 \times 56 \times 3.5$  in kpc so the plotted distortions from planarity exaggerate the true distortions. The mean radii of the rings shown in this figure are: 4.37, 7.88, 11.38, 14.87, and 18.35 kpc.

angle less than  $7^\circ$ .

## 6 SATELLITE SINKING AND DISRUPTION TIMES

In order to verify the reliability of the decay rate and disruption time of the satellites in our simulations we built up a self-consistent model called 'NEW' similar to our model

G1S3 but with only a fourth of the number of particles in each of the components present in the model. The mass evolution and disruption rate of the satellite for these models are shown in figure 10(a)-(b) where the open circles represent model G1S3 and the open squares joined by solid lines correspond to the 'NEW' model. Notice that the agreement is good with differences in the disruption process of the satellite being more evident in the last stages of its evolution.

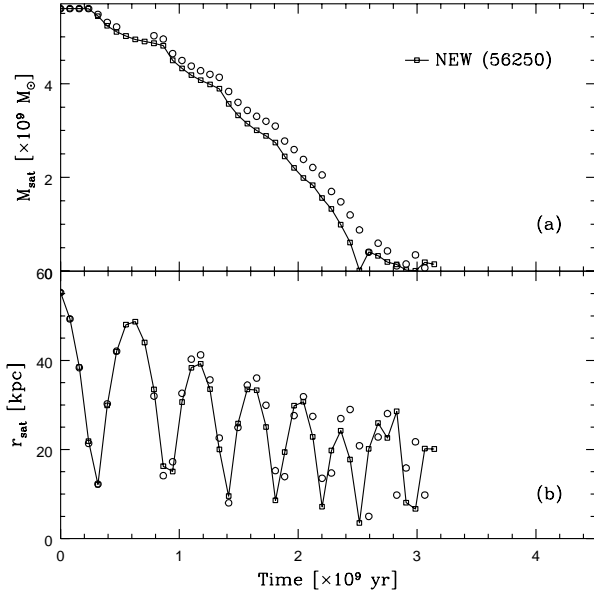


**Figure 10.** (a) This figure shows the mass of the satellite as a function of time. In both models G1S3 (open circles) and NEW we obtained similar times for the total disruption of the satellite which occurs about 2.6–2.8 Gyr. (b) The satellite position is presented as a function of time. Notice that the satellite is completely destroyed before it reaches the centre of the galaxy.

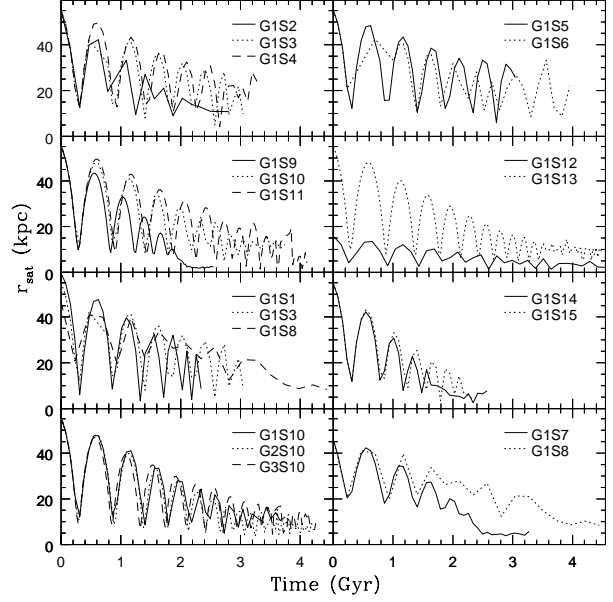


**Figure 12.** The orbital decay rate for the satellites in most of our simulations.

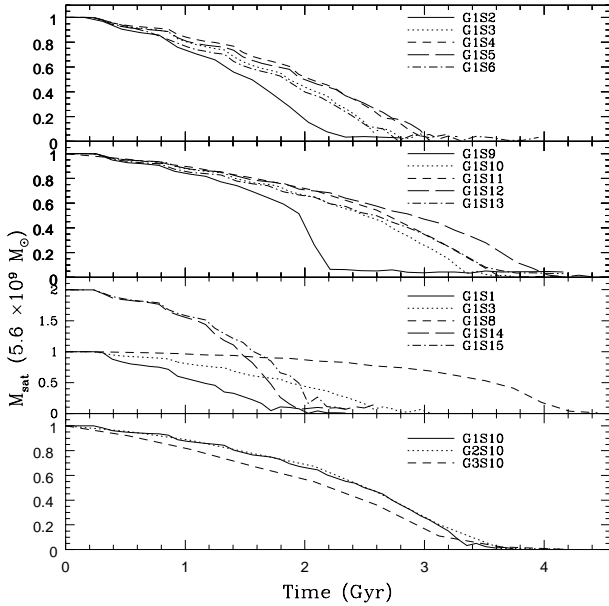


**Figure 11.** The disruption times of the satellites for most of our simulations. Most of the damage to the satellites occurs at pericentre since the tidal force due to the galactic potential is strongest there.

As the satellite is being accreted by the host galaxy, there are two main physical mechanisms that regulate its evolution: the tidal interaction and dynamical friction. Figures 11 and 12 show the effects of these mechanisms in the overall evolution of the satellites for most of our simulations. These effects are illustrated by our model G1S1. Notice that the biggest ‘jumps’ in the mass evolution of the satellite correspond to its passage through pericentre. This is easily understood since at that position the tidal interaction of the satellite with the host galaxy is the strongest since the gradient of the galactic gravitational force reaches a maximum at pericentre. Comparison of the different models yields the following conclusions: (i) for a given circularity and satellite model, the disruption of the satellite occurs faster for prograde orbits than for retrograde ones being more evident for coplanar orbits. Furthermore, just from the mass loss and disruption total times, it is difficult to distinguish between polar and retrograde orbits. In the case of prograde orbits, the satellites suffer a faster disruption and sinking if they follow orbits which are closer to coplanar. (ii) For a given orbit, the decay rate and disruption of our satellite with an initial mass of  $0.2 M_D$  are faster than for the satellite with an initial mass of  $0.1 M_D$  since the decay rate is proportional to the satellite mass. (iii) For a given satellite mass and orbit a more compact satellite survives for a longer time than a less compact one since its binding energy is greater. (iv) Finally, although we do not have a large number of simulations, we note that, for a given satellite, the disruption time scales roughly as  $\epsilon_j^{1/3}$ .

## 7 CHANDRASEKHAR'S DYNAMICAL FRICTION FORMULA

In this section we briefly address the reliability of Chandrasekhar's dynamical friction formula (Chandrasekhar 1960) for describing the decay rate of the satellites in our N-body simulations. To carry out this study, we built up a galaxy model similar to our fully self-consistent one but replacing the self-gravitating halo by a rigid potential which is free to move in response to the particle distribution of the other components. For a Maxwellian distribution of velocities with a dispersion velocity  $\sigma(r)$  we have that the dynamical friction on the satellite is given by (Binney and Tremaine 1987):

$$\mathbf{F}_{df} = -\frac{4\pi \ln \Lambda G^2 M_S^2 \rho_H(r)}{v_S^3} \left[ \operatorname{erf}(X) - \frac{2X}{\sqrt{\pi}} e^{-X^2} \right] \mathbf{v}_S, \quad (6)$$

where  $X \equiv v_S/(\sqrt{2}\sigma(r))$  and  $\ln \Lambda$  is the Coulomb logarithm. The basic underlying assumption in the derivation of this equation is that a point particle of mass  $M_S$  moves with a velocity  $\mathbf{v}_S$  in an homogeneous and infinite background of lighter particles whose self-gravity is completely ignored. As this point particle travels across the background it deflects particles (gravitational focusing) producing a density enhancement (a wake) behind it which is responsible for the drag force expressed in equation (6) (Mulder 1983). Obviously, the manifestation of this force requires a halo made of independent particles and hence, it will be not present in a rigid model. Since we want to check the reliability of equation (6) to describe the sinking rate in our self-consistent simulations we have introduced it 'by hand' in the case of the rigid halo models to emulate a drag force acting on the satellite. This will allow us to determine the importance of the self-gravity of the background particles of the halo particles to the sinking process. We should remark that the disc was kept alive and, hence, 'disc friction' is included.

In addition to the study of the orbital decay of satellites within their host galaxies (e.g. QG, QHF) dynamical friction has been invoked to explain the evolution of cD galaxies in clusters of galaxies (Ostriker and Tremaine 1975, White 1976) as well as the formation of galactic nuclei (Tremaine, Ostriker and Spitzer 1975). Despite numerous studies, there is still disagreement about the applicability of Chandrasekhar's relation in such situations and the relevance of its inherent local character. Thus, Lin and Tremaine (1983) using a semi-restricted N-body code found that equation (6) provides accurate decay rates for satellites following circular orbits for a large part of the parameter space (satellite mass, satellite size, and number density and mass of halo stars) suggesting that the self-gravity of the halo stars is unimportant. In contrast, White (1983) using fully self-consistent N-body calculations based on a spherical harmonics expansion found that a local description of the dynamical friction was not enough to determine the sinking times in satellites. However, Bontekoe and van Albada (1987) reached a conclusion more in agreement with Lin and Tremaine (1987) since they found that higher order terms of the harmonic expansion had no discernible effect on their results. In an attempt to clarify this situation, Zaritsky and White (1988) carried out an exhaustive study using several codes and found that the self-gravity of the halo is not

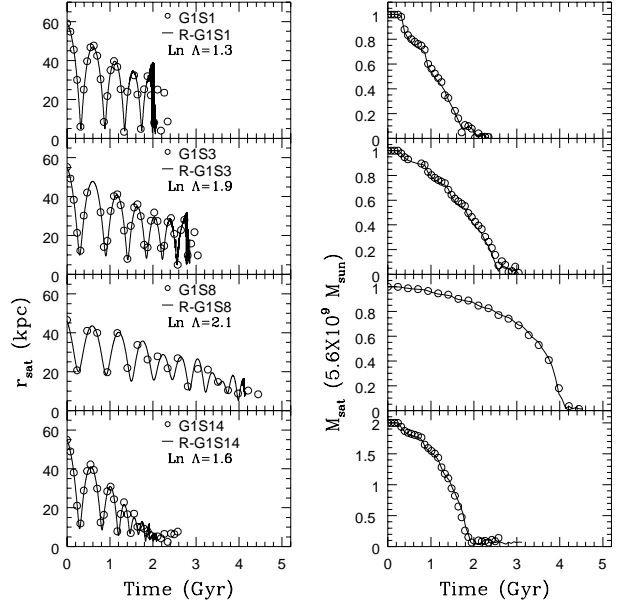


**Figure 13.** Decay and disruption rates for a few of our models. Open circles corresponds to our fully self-consistent simulations while solid lines represent the same model but with a rigid halo free to move instead. Dynamical friction has been computed using Chandrasekhar's relation.

important for the sinking rate of the satellite. Also, Hernquist and Weinberg (1989) used self-consistent and semi-restricted N-body algorithms to study this problem and to try to understand the discrepancy. They concluded that orbital decay is strongly suppressed if self-gravity of the response is taken into account in disagreement with Zaritsky and White (1988). Since most of the previous work was restricted to satellites following circular orbits, Séguin and Dupraz (1994, 1996) employed a semi-restricted method to determine the applicability of Chandrasekhar's relation to head-on encounters. They also conclude that the global response of the galaxy cannot be ignored.

Due to this confusion about the role played by the global response of the halo in the sinking process of the satellite we have repeated four of our simulations (models G1S1, G1S3, G1S8 and G1S14) but replacing the self-consistent halo by a rigid one which is free to move. With these new simulations we try to cover several situations (different eccentricities and satellite masses) to see whether the expression (6) deviates from the results in our self-consistent N-body calculations and from a satellite that does not follow a circular orbit as is claimed by Séguin and Dupraz (1994, 1996). Figure 13 shows the sinking and disruption times for the satellites in the new simulations. Open squares represent the fully self-consistent simulations while solid lines correspond to the model with rigid haloes. To quantify the sinking and disruption rates we have used equation (6) with  $\rho_H(r) = \rho(r)$  representing the local halo density at the satellite position and the satellite mass  $M_S = M_S(t)$  as the particles that remain bound.  $\mathbf{F}_{df}$  is applied to all the bound particles. Notice that the agreement is quite remarkable and it suggests that a local description, as is implicit in Chandrasekhar's

**Table 6.** Disc kinematical changes. Rigid haloes

Model	$R_c^*$			$R_\bullet$			$R_4^\dagger$		
	$(\Delta\sigma_R, \Delta\sigma_\phi, \Delta\sigma_z)$	$\Delta Q$	$\Delta z_o$	$(\Delta\sigma_R, \Delta\sigma_\phi, \Delta\sigma_z)$	$\Delta Q$	$\Delta z_o$	$(\Delta\sigma_R, \Delta\sigma_\phi, \Delta\sigma_z)$	$\Delta Q$	$\Delta z_o$
R-G1S1	(9, 6, 4)	0.4	50	(5, 4, 5)	0.4	200	(10, 9, 8)	2.6	550
R-G1S3	(9, 6, 5)	0.3	50	(5, 4, 5)	0.4	150	(13, 8, 10)	2.2	750
R-G1S8	(9, 8, 6)	0.3	50	(10, 5, 5)	0.6	250	(20, 15, 16)	2.8	1000
R-G1S14	(27, 16, 13)	0.5	150	(26, 16, 30)	1.8	1200	(30, 23, 28)	3.4	1700

As in Table 4, symbols \* and † denote quantities at the centre and  $4R_D$ , respectively.

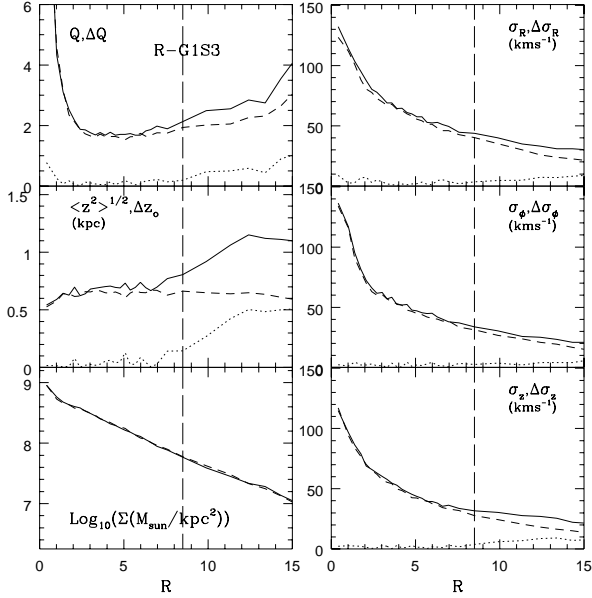


**Figure 14.** Disc kinematics for model R-GS3 (solid lines). Dashed lines represent the kinematics of the equivalent isolated galaxy model while dotted lines correspond to the changes suffered by the disc as a consequence of the satellite accretion.

formula, is adequate to determine the sinking times of satellites whenever the satellite is immersed in the halo provided we choose the right value for  $\Lambda$  and we define the satellite mass  $M_S$  as the total mass of bound particles. The values for  $\Lambda$  that appear in figure 13 were estimated initially from the expression  $\Lambda = p_{max}/p_{min}$  † and afterwards were fine-tuned to get the ‘right’ values. We must point out that to determine the dependence of  $\Lambda$  on the orbital parameters and the satellite structure further work is necessary.

† Here,  $p_{max}$  and  $p_{min}$  are the maximum and minimum impact parameter, respectively, and are defined by  $p_{max} \equiv \langle R \rangle \simeq GM^2/(2|W|)$  and  $p_{min} \equiv GM_S/\sigma_H^2(r_p)$  where  $M$ ,  $|W|$ ,  $M_S$ ,  $\sigma_H(r_p)$  are the total mass of the spiral galaxy, the total potential energy of the spiral, the satellite’s initial mass and the one-dimensional dispersion velocity of the halo evaluated at the pericentric radius  $r_p$ , respectively.

## 8 RIGID HALOES AND DISC HEATING AND THICKENING

We have carried out a detailed analysis of the simulations involving rigid haloes in order to address the importance of the self-consistent representation of the haloes in the accretion of a satellite. In figure 14 we show the resulting disc kinematics (solid lines) for the case equivalent to our model G1S3 but with a rigid halo (model R-G1S3). The kinematics of the corresponding isolated control model is displayed in the same figure (dashed lines) and the kinematical changes induced by the accretion event are indicated by dotted lines. From comparison of figures 5 and 14 we can notice that: (i) the disc thickening due purely to numerical relaxation has been diminished by the introduction of a rigid halo; in an isolated model the disc heating is dominated by encounters between disc and halo particles. (ii) After completion of the accretion event, the radial and azimuthal changes of the velocity ellipsoid induced by the satellite are roughly similar to those found in model G1S3. Thus, limits on accreted mass based only on the value of  $\Delta Q$  ( $\propto \Delta\sigma_R$ ) and ignoring any change of  $\Sigma_D(R)$  and any gas cooling will be essentially the same even if the spherical halo is represented by a rigid potential rather than by a distribution of particles provided the decay and disruption rates of the satellite are considered adequately (in our case by equation 6). (iii) However, the response of the vertical structure of the disc seems to be strongly coupled to the responsiveness of the halo. For example, for model R-G1S3 we found that the change of the vertical scale length at 14 kpc is about a factor of 2 bigger than in model G1S3 while at the solar radius the factor is  $\sim 1.5$ . This difference is substantial despite the fact that we have mimicked the satellite’s orbital energy loss to the rigid halo through equation 6. This may be because the disc develops some other instabilities, as satellite accretion proceeds, which can be damped by a self-gravitating halo. (iv) As the satellite becomes more massive, the necessity of a self-consistent treatment of the halo is more evident; see figure 15 which is the equivalent of our model G1S14 (compare it with figure 6). The kinematics of this set of simulations using rigid haloes is summarized in Table 6.

## 9 CONCLUSIONS

We can summarize our main conclusions as follows:

- A comparison of our results with those obtained using

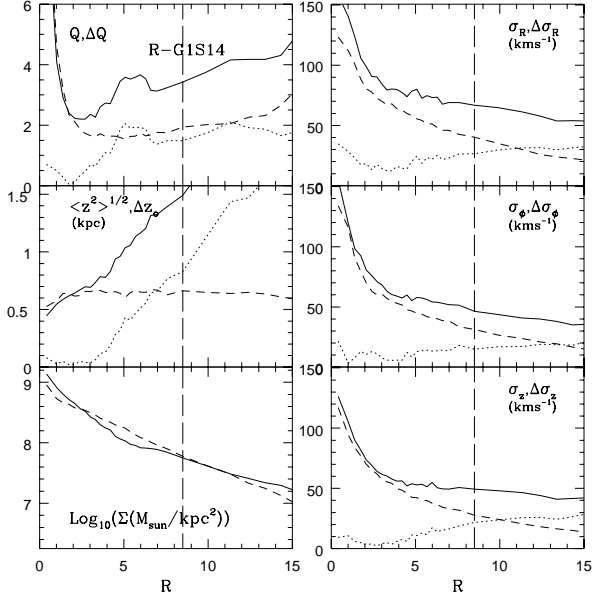


**Figure 15.** The same as figure 14 but for a satellite with  $0.2 M_D$ .

TO's formulae shows that the mass limits they derived are too strict. In general, TO tend to overestimate the damaging effects of satellite accretion by a factor of about 2 – 3 at the Solar radius. The damaging effects in our simulations may also be an overestimation since we ignore any contribution of gas cooling during the accretion process. The origin of the discrepancy between TO's predictions and our results may lie in the fact that: (i) their analysis ignores the coherent response of the disc and its interaction with the halo. (ii) Their assumption that the satellite's orbital energy is deposited locally in the disc is clearly unrealistic. (iii) A fully self-consistent treatment of the dynamics is needed to get reliable results. A rigid halo (with dynamical friction introduced through equation (6) leads to a larger increase of the vertical scale length of the disc by a factor of 1.5 – 2. A self-consistent treatment is more important for more massive satellites.

- The damaging effects (heating and thickening) on the disc are very different for satellites on prograde and retrograde orbits. A satellite on a prograde orbit tends to heat the stellar disc while its retrograde counterpart induces a coherent response of the disc in a form of a tilt. A massive satellite on a retrograde orbit may be accreted by a spiral galaxy without destroying its disc. Furthermore, a massive central bulge may reduce the vertical heating of the disc for prograde orbits (but weaker for retrograde) while it may slightly diminish the tilting of the disc for retrograde ones (but not for prograde).

- A satellite as massive as  $0.1 M_D$  and moving in a roughly elongated orbit (e.g. our model G1S3) does not produce a strong stellar warp. The most noticeable case of warp formation occurs in our model G1S14 where we see a departure from the disc plane of less than  $7^\circ$  in the outer regions (at about 15 kpc).

- Chandrasekhar's dynamical friction formula gives remarkably good estimates for the sinking and disruption rates of satellites in a variety of situations provided a suitable

value is chosen for the Coulomb logarithm and the satellite mass is taken to be the mass still bound to the satellite at each moment.

## 10 ACKNOWLEDGMENTS

We thank L. Hernquist for provide us with his algorithms. We also thanks an anonymous referee for his helpful comments to improve this paper. HV acknowledges useful conversations with L. Aguilar and S. Levine. HV thanks CONA-CyT (Consejo Nacional de Ciencia y Tecnología) of México for a studentship and the Max-Planck für Astrophysik for a Stipendium for the fulfillment of this research. Most of the simulations were run at the Max-Planck Society's Computer Centre at Garching, Germany.

## REFERENCES

- Aarseth S. J., Fall S. M., 1980, *ApJ*, 236, 43  
 Bahcall J.N., Schmidt M., Soneira R.M., 1982, *ApJ*, 258, L23  
 Barnes J. E., 1996, in Morrison H. and Sarajedini A., eds., *ASP Conf. Ser. Vol. 92, Formation of the Galactic Halo ... Inside and Out*, p. 415  
 Barnes J. E., 1992, *ApJ*, 393, 484  
 Barnes J. E., Hut P., 1986, *Nat*, 324, 446  
 Bender R., Burstein D., Faber S. M., 1992, *ApJ*, 399, 462  
 Binggeli B., Cameron L. M., 1991, *A&A*, 252, 27  
 Binney J., 1992, *ARA&A*, 30, 51  
 Binney J., Tremaine S., 1987, *Galactic Dynamics*, Princeton University Press  
 Bontekoe Tj. R., van Albada T. S., 1987, *MNRAS*, 224, 349  
 Briggs F., 1990, *ApJ*, 352, 15  
 Carlberg R. G., Couchman H. M. P., 1989, *ApJ*, 340, 47  
 Carlberg R. G., Pritchett, C. J., Infante, L., 1994, *ApJ*, 435, 510  
 Carney B., Latham D. W., 1987, in Kormendy J., Knapp G. R., eds, *Proc. IAU Symp. 117, Dark Matter in the Universe*. Reidel, Dordrecht, p. 39  
 Chandrasekhar S., 1960, *Principles of Stellar Dynamics*, New York, Dover Publications  
 Courteau S., 1997, *AJ*, 114, 2402  
 Dressler A., Shectman S. A., 1988, *AJ*, 95, 985  
 Dubinski J., Carlberg R. G., 1991, *ApJ*, 378, 496  
 Dubinski J., Kuijken K., 1995, *ApJ*, 442, 492  
 Evrard A. E., Summers F. J., Davis M., 1994, *ApJ*, 422, 11  
 Freeman K. C., 1996, in Morrison H. L., Sarjedini A., eds, *ASP Conf. Ser. Vol. 92, Formation of the Galactic Halo ... Inside and Out*, p. 3  
 Frenk C. S., White S. D. M., Davis M., Efstathiou G., 1988, *ApJ*, 327, 507  
 Henderson A. P., Jackson P. D., Kerr F. J., 1982, *ApJ*, 263, 116  
 Hernquist L., 1987, *ApJS*, 64, 715  
 Hernquist L., 1990, *ApJ*, 356, 359  
 Hernquist L., 1993, *ApJS*, 86, 389  
 Hernquist L., Weinberg M. D., 1989, *MNRAS*, 238, 407  
 Huang S., Carlberg R. G., 1997, *ApJ*, 480, 503  
 Jones C., Forman W., 1992, in Fabian A. C., ed., *Clusters and Superclusters of Galaxies*. Kluwer, Dordrecht, p. 49  
 Kauffmann G., White S. D. M., 1993, *MNRAS*, 261, 921  
 King I. R., 1966, *AJ*, 71, 65  
 Lacey C. G., Cole S., 1993, *MNRAS*, 262, 627  
 Lewis J. R., Freeman K. C., 1989, *AJ*, 97, 139  
 Lin D. N. C., Tremaine S., 1983, *ApJ*, 264, 364  
 Mihos C., Hernquist L., 1994, *ApJ*, 425, L13  
 Moore B., 1994, *Nature*, 370, 209

- Morrison H. L., 1996, in Morrison H. L., Sarjedini A., eds, ASP Conference Series, Vol. 92, Formation of the Galactic Halo ... Inside and Out, p. 453
- Mulder W. A., 1983, *A&A*, 117, 9
- Navarro J. F., Frenk C. S., White S. D. M., 1994, *MNRAS*, 267, L1
- Navarro J. F., Frenk C. S., White S. D. M., 1995, *MNRAS*, 275, 56
- Negroponte J., White S. D. M., 1983, *MNRAS*, 205, 1009
- Nelson R. W., Tremaine S., 1995, *MNRAS*, 275, 897
- Ostriker J. P., 1990, in Kron R. G., ed, ASP Conf. Ser. Vol. 10, Evolution of the Universe of Galaxies. Astron. Soc. Pac., San Francisco, p. 23
- Ostriker J. P., Tremaine S., 1975, *ApJ*, L113
- Persic M., Salucci P., Stel F., 1996, *MNRAS*, 281, 27
- Quinn P. J., Goodman J., 1986, *ApJ*, 309, 472
- Quinn P. J., Hernquist L., Fullagar D., 1993, *ApJ*, 403, 74
- Richstone D., Loeb A., Turner E. L., 1992, *ApJ*, 393, 477
- Sánchez-Saavedra M. L., Battaner E., Florido E., 1990, *MNRAS*, 246, 458
- Schweizer F., 1990, in Wielen R., ed., Dynamics and Interactions of Galaxies, Berlin:Springer, p. 60
- Séguin P., Dupraz C., 1994, *A&A*, 290, 709
- Séguin P., Dupraz C., 1996, *A&A*, 310, 757
- Sellwood J. A., Wilkinson A., 1993, *Rep. Prog. Phys.*, 56, 173
- Silk J., Wyse R. F. G., 1993, *Physics Reports*, 231, 293
- Sofue Y., Tutui Y., Honma M., Tomita A., 1997, *AJ*, 114, 2428
- Sparke L. S., Casertano S., 1988, *MNRAS*, 234, 873
- Spitzer L., 1942, *ApJ*, 95, 329
- Toomre A., 1977, in Tinsley B. M. and Larson R. B., eds., The Evolution of Galaxies and Stellar Populations, Yale Univ, Obs., New Haven, p. 401
- Tóth G., Ostriker J.P., 1992, *ApJ*, 389, 5
- Tremaine S., Ostriker J. P., Spitzer L., 1975, *ApJ*, 196, 407
- Vader J. P., Chaboyer B., 1994, *AJ*, 108, 1209
- Walker I. R., Mihos C., Hernquist L., 1996, *ApJ*, 460, 121
- Weinberg M. D., 1996, *ApJ*, 455, 131
- White S. D. M., 1976, *MNRAS*, 174, 19
- White S. D. M., 1983, *ApJ*, 274, 53
- Zaritsky D., White S. D. M., 1988, *MNRAS*, 235, 289
- Zaritsky D., Olszewski E. W., Schommer R. A., Peterson R. C., Aaronson M., 1989, *ApJ*, 345, 759
- Zaritsky D., White S. D. M., 1994, *ApJ*, 435, 599

This figure "Fig03.jpg" is available in "jpg" format from:

<http://arxiv.org/ps/astro-ph/9809412v1>

This figure "Fig04.jpg" is available in "jpg" format from:

<http://arxiv.org/ps/astro-ph/9809412v1>

This figure "Fig09.jpg" is available in "jpg" format from:

<http://arxiv.org/ps/astro-ph/9809412v1>